Discover Nano

Research

Nanovoid formation mechanism in nanotwinned Cu

Cuncai Fan[1] · Haiyan Wang[2,3] · Xinghang Zhang[2]

Received: 30 December 2023 / Accepted: 27 February 2024
Published online: 12 March 2024
© The Author(s) 2024 OPEN

Abstract
Nanotwinned metals have been intensely investigated due to their unique microstructures and superior properties. This work aims to investigate the nanovoid formation mechanism in sputter-deposited nanotwinned Cu. Three different types of epitaxial or polycrystalline Cu films are fabricated by magnetron sputtering deposition technique. In the epitaxial Cu (111) films deposited on Si (110) substrates, high fractions of nanovoids and nanotwins are formed. The void size and density can be tailored by varying deposition parameters, including argon pressure, deposition rate, and film thickness. Interestingly, nanovoids become absent in the polycrystalline Cu film deposited on Si (111) substrate, but they can be regained in the epitaxial nanotwinned Cu (111) when deposited on Si (111) substrate with an Ag seed layer. The nanovoid formation seems to be closely associated with twin nucleation and film texture. Based on the comparative studies between void-free polycrystalline Cu films and epitaxial nanotwinned Cu films with nanovoids, the underlying mechanisms for the formation of nanovoids are discussed within the framework of island coalescence model.

Keywords Magnetron sputtering · Nanotwinned metals · Nanovoids · Epitaxial film

1 Introduction

As a typical method of physical vapor deposition (PVD), magnetron sputtering technique is attractive to industry for fabricating various metallic films and coatings with unique microstructures and properties [1]. Sputtering deposition normally takes place in a vacuum chamber where the atomic flux of source material is transferred from the target (cathode) to the substrate (anode) [2]. Since this process is largely nonequilibrium, involving the sputtering of a target by energetic ions (e.g., Ar ions) and the condensation of a vapor into a solid, as-deposited films can be far away from their energetic minimums [3]. As a result, the microstructure of sputter-deposited coatings is characterized by a large number of defects, such as grain boundaries and voids [4]. For instance, previous studies have revealed that the polycrystalline metallic films synthesized by sputtering at low temperatures consist of fine grains ranging from several to tens of nanometers in size [5]. Especially, in sputter-deposited films of face-centered-cubic (FCC) metals with a low stacking fault energy, such as copper (Cu), silver (Ag), and 330 steel [6–8], a considerable fraction of nanoscale growth twins can be formed. The twin structures are bounded by a special type of high-angle grain boundary, the coherent twin boundary (CTB) that stores a minimal boundary energy and renders nanotwinned (NT) metals superior physical and mechanical properties [9, 10]. Compared with nanograined and coarse-grained counterparts, the NT metals exhibit combinations of high electrical conductivity [11, 12], good thermal stability [13–15], outstanding radiation tolerance [16–19], as well as high strength and ductility [20, 21]. Recently, it has been

✉ Cuncai Fan, cuncafan@cityu.edu.hk; ✉ Xinghang Zhang, xzhang98@purdue.edu | [1]Department of Mechanical Engineering, City University of Hong Kong, Kowloon, Hong Kong, China. [2]School of Materials Engineering, Purdue University, West Lafayette, IN 47907, USA. [3]School of Electrical and Computer Engineering, Purdue University, West Lafayette, IN 47907, USA.

found that the mechanical properties of NT metal films can be enhanced further by introducing nanovoids [22, 23]. Our previous studies also found that preexisting nanovoids can improve the radiation tolerance of NT metals [24–26], as they can act as the effective sinks for radiation-induced defects [27, 28]. Although the effects of nanovoids on mechanical and radiation properties have been systematically investigated, the underlying mechanism of nanovoid formation in NT films is still unclear. To advance the applications of NT metals in surface and coatings technology and to extend our understandings on the sputtered nanostructured materials, it is warranted to investigate how nanovoids form and evolve during film growth.

This work focuses on the nanovoid evolution in sputter-deposited NT and polycrystalline Cu films. The variations of nanovoid size and density with increasing Ar working pressure, deposition rate, and film thickness were systematically investigated. Experimental results revealed that the nanovoid formation is closely associated with twin nucleation and film texture, hence this study provides new insights into design and fabrication of NT metallic films with nanovoids.

2 Experimental

High purity (99.995%) Cu thin films were deposited onto the HF-etched silicon (Si) wafers at room temperature using a custom-designed direct current magnetron sputtering system. Prior to depositions, the main chamber was pumped to a typical base pressure $< 8 \times 10^{-8}$ torr. Sputtered films can be divided into three types according to the variations of deposition condition, orientation of Si substrate, and the seed layer on Si substrates. Type 1 films were directly deposited on Si (110) substrates. They include three subgroups with different Ar working pressures P_{Ar}, deposition rates $R_{Dep.}$, and film thicknesses T_{Flim}, as summarized in Table 1. In contrast, Types 2 and 3 refer to the Cu films deposited on Si (111) substrates, respectively, without and with an Ag seed layer (~ 200 nm thick); they have the same Ar working pressure (~ 2.6 mtorr), deposition rate (~ 1 nm/s), and total film thickness (~ 2 µm). The deposition rate in each sample was controlled by changing Ar working pressure and sputtering power.

The X-ray diffraction (XRD) analyses of as-deposited films were performed by a Panalytical Empyrean X'pert PRO MRD X-ray diffractometer with a Cu Kα1 source. The film surface was characterized by an FEI Nova NanoSem 450 scanning electron microscope (SEM) operated at 20 kV. Plan-view and cross-section transmission electron microscope (TEM) specimens were prepared by polishing, dimpling, and low energy Ar ion milling. All the TEM specimens were subsequently examined by an FEI Talos 200X TEM operated at 200 kV. Besides, the Si substrate radii, R_0 and R_1 before and after film deposition, were measured using a profilometer, and film residual stress σ was calculated based on the Stoney formula [29]

$$\sigma = \frac{M_s T_{Si}^2}{6T_{Film}} \left(\frac{1}{R_1} - \frac{1}{R_0} \right) \tag{1}$$

where T_{Si} is the Si substate thickness (~ 500 µm), and M_s is the biaxial modulus of the substrate, ~ 217 GPa for Si (110) [30].

Table 1 Sputtering conditions, microstructures, and residual stress of the Type 1 NT–NV Cu (111) films grown on Si (110) substrates

Sample label	Deposition conditions			Microstructures				Film residual stress σ (MPa)
	P_{Ar} (mtorr)	$R_{Dep.}$ (nm/s)	T_{Flim} (µm)	D (nm)	t (nm)	V (nm)	ρ_V (10^{-4} nm^2)	
a1_1.7 mtorr	1.7	0.6	2.2	120 ± 27	7 ± 4	6 ± 2	3.4 ± 0.5	581 ± 1
a2_3.6 mtorr	3.6	0.6	2.2	94 ± 21	6 ± 2	5 ± 2	6.6 ± 0.4	604 ± 5
a3_5.5 mtorr	5.5	0.6	2.1	94 ± 22	8 ± 4	5 ± 1	12.9 ± 1.0	528 ± 4
b1_0.2 nm/s	2.6	0.2	2.0	123 ± 16	7 ± 6	7 ± 3	2.1 ± 0.2	836 ± 40
b2_1.3 nm/s	2.6	1.3	2.3	120 ± 19	8 ± 5	5 ± 1	5.5 ± 0.4	654 ± 30
b3_2.9 nm/s	2.6	2.9	2.1	115 ± 20	5 ± 3	6 ± 2	8.5 ± 0.7	822 ± 63
c1_1.2 µm	2.6	0.6	1.2	91 ± 14	5 ± 3	5 ± 3	8.8 ± 0.5	690 ± 60
c2_2.5 µm	2.6	0.6	2.4	115 ± 19	6 ± 2	6 ± 2	5.0 ± 0.4	561 ± 2
c3_6.5 µm	2.6	0.6	6.5	180 ± 24	26 ± 22	14 ± 5	0.9 ± 0.1	424 ± 6

P_{Ar} Ar pressure, $R_{Dep.}$ deposition rate, T_{Flim} film thickness, D domain size, t twin spacing, V void size, ρ_V void density, σ film residual stress

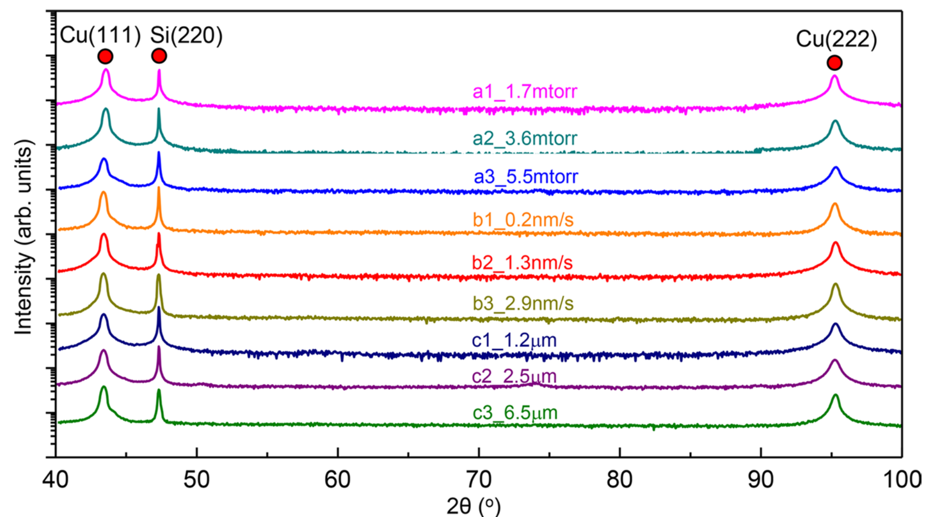

Fig. 1 (Color online) The XRD 2θ-scan profiles of Cu films directly deposited on Si (110) substrates. The existence of only Cu (111) and (222) suggests the formation of epitaxial films along growth direction. The spectra correspond to the samples synthesized with increasing argon working pressure from 1.7 to 5.5 mtorr (a1)–(a3), increasing deposition rate from 0.2 to 2.9 nm/s (b1)–(b3), and increasing film thickness from 1.2 to 6.5 μm (c1)–(c3). The samples are summarized in Table 1

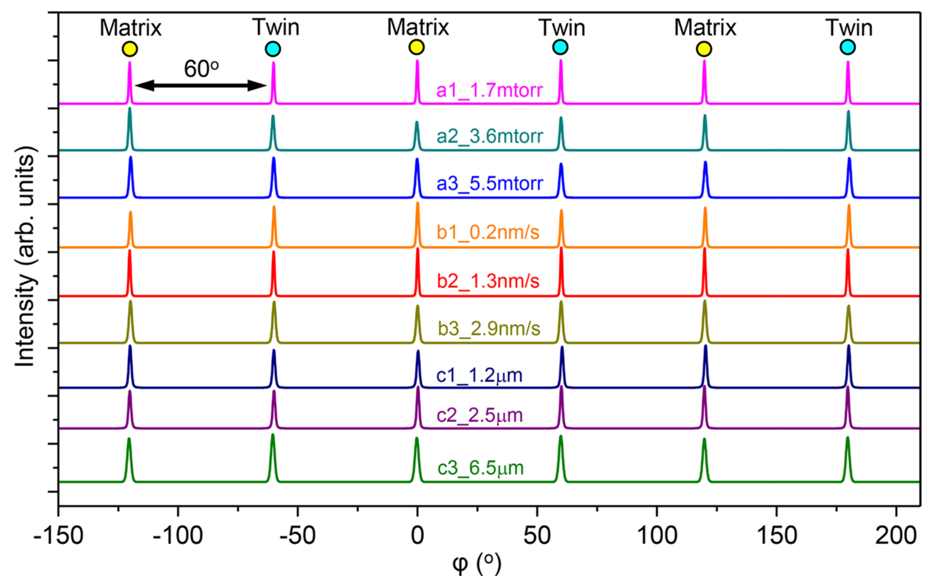

Fig. 2 (Color online) The XRD φ-scan profiles of Cu {111} with a six-fold symmetry indicating the formation of high-density growth twins in as-deposited films

3 Results

3.1 Type 1: nanovoid–nanotwinned Cu (111) directly deposited on Si (110) in different deposition conditions

Following our previous studies [24, 25], we first investigated the effects of sputtering condition parameters on the evolutions of texture of Cu films directly deposited on Si (110) substrates. Figure 1 compiles the normal XRD 2θ-scan profiles of as-deposited films. Apart from Si (220), the X-ray spectra only show two strong peaks, namely Cu (111) and Cu (222), indicating the formation of epitaxial Cu (111) films in all cases, regardless of the variation of Ar pressure from 1.7 to 5.5 mtorr, the increasing deposition rate from 0.2 to 2.9 nm/s, and the increasing film thickness from 1.2 to 6.5 μm. The corresponding XRD φ-scan profiles of Cu {111} in Fig. 2 show strong peaks with a six-fold symmetry. These peaks must arise from two sets of variants with a 60° rotation angle along the out-of-plane direction, that is the Cu <111> crystallographic direction, indicating the formation of a significant fraction of growth twins in sputtered Cu films.

The plan-view TEM micrographs of as-deposited Cu films in Fig. 3 show that the films contain polygonal domains, and there are abundant nanovoids randomly distributed along domain boundaries. Moreover, the inset selected area diffraction (SAD) patterns demonstrate the formation of single crystal-like grains oriented along <111> direction, consistent

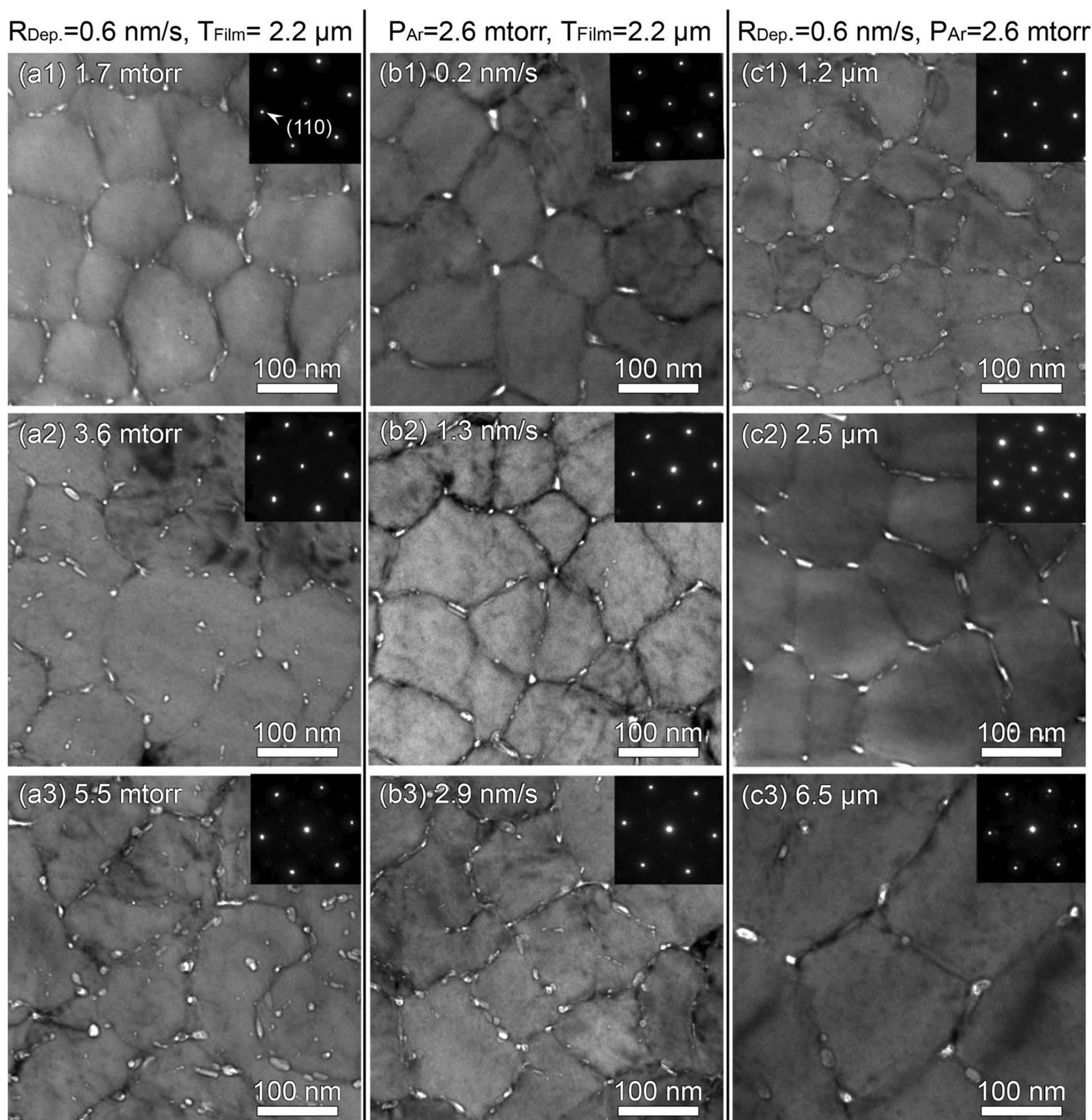

Fig. 3 Plan-view TEM micrographs displaying abundant nanovoids that are mostly distributed along domain boundaries. The inset SAD patterns clearly show single crystal-like diffraction along the Cu <111> zone axis

with the XRD profiles presented in Fig. 1. The cross-section TEM micrographs in Fig. 4 show columnar domains consisting of high-density CTBs. These boundaries appear every few nanometers and are normal to the film growth direction. The inset SAD patterns confirm the formation of growth twins, also in good agreement with the *φ*-scan profiles in Fig. 2. Since the NT samples have abundant nanovoids, hereafter we will refer to them as nanovoid–nanotwinned (NV–NT) Cu.

It seems that varying deposition parameters can hardly change the texture of NV–NT Cu film. Other microstructure features indeed vary, including twin spacing, void size and density, as well as domain size. As shown in Fig. 5a–c, the twin spacing t, void size V, and domain size D fluctuates slightly with varying Ar pressure P_{Ar} and deposition rate $R_{Dep.}$. However, t, V and D all enlarge with increasing film thickness T_{Flim}. This variation could be caused by annealing, as it takes a longer time to deposit a thicker film when heat cannot be transferred instantly from Si wafer. It is worth noting that the void size V is comparable to the twin spacing t. This aspect will be discussed later in more detail. It is also noted that the void density, ρ_V changes prominently with deposition conditions. As shown in Fig. 5d–f, ρ_V increases with increasing P_{Ar} and $R_{Dep.}$, but it decreases with increasing T_{Flim}. The variation of void density with deposition conditions were also reported elsewhere [31].

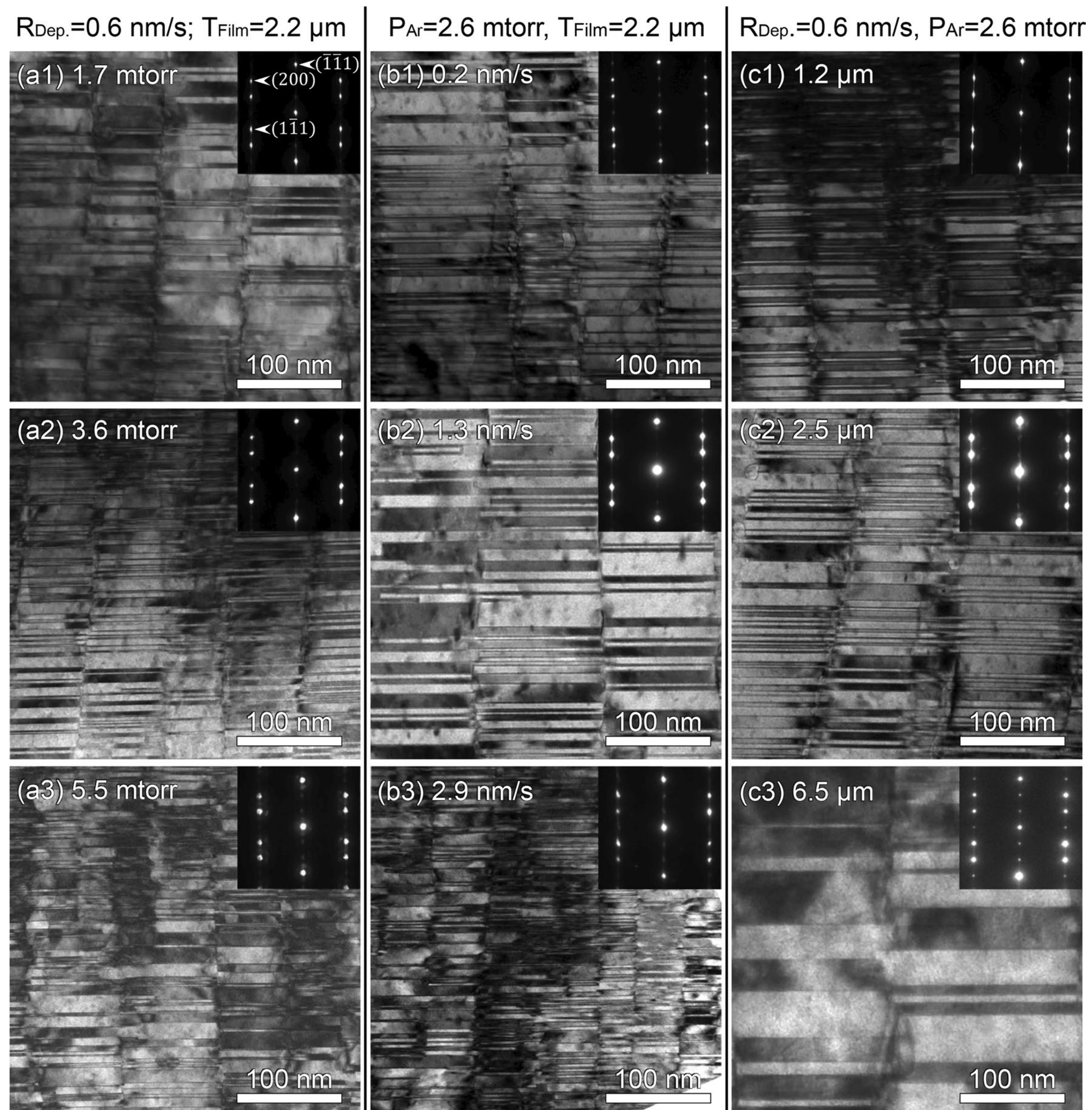

Fig. 4 Cross-section TEM micrographs captured from Cu <110> zone axis, revealing columnar domains and high-density growth twins in epitaxial Cu (111) films. The inset SAD patterns confirm the formation of twin structures

The evolutions of film residual stress σ are plotted in Fig. 6. All films have tensile stresses, ranging from 0.4 to 0.9 GPa. Like microstructure features, the residual stress also exhibits a complex dependence on deposition parameters. Detailed statistics on the evolutions of microstructures and residual stresses are summarized in Table 1.

3.2 Type 2: poly-crystalline Cu deposited on Si (111) substrate without seed layer

The texture and microstructure of sputtered Cu film can be substantially modified by changing the orientation of single crystal Si substrate. Figure 7 illustrates a polycrystalline Cu deposited on HF-etched Si (111). The 2θ-scan profile in Fig. 7a shows the existence of several peaks arising from a couple of crystallographic planes of Cu, including (100), (111), (110), and (113). This XRD pattern indicates the formation of polycrystalline grains in as-deposited film. The plan-view TEM micrograph and the inset ring-like SAD pattern presented in Fig. 7b also confirm the formation of polycrystalline Cu. The as-deposited Cu shows a bimodal grain size distribution, with large grain size on the order of 1 μm and small grains less than 100 nm. The enlarged TEM image in Fig. 7c reveals the nanograins are roughly equiaxed without nanovoids at

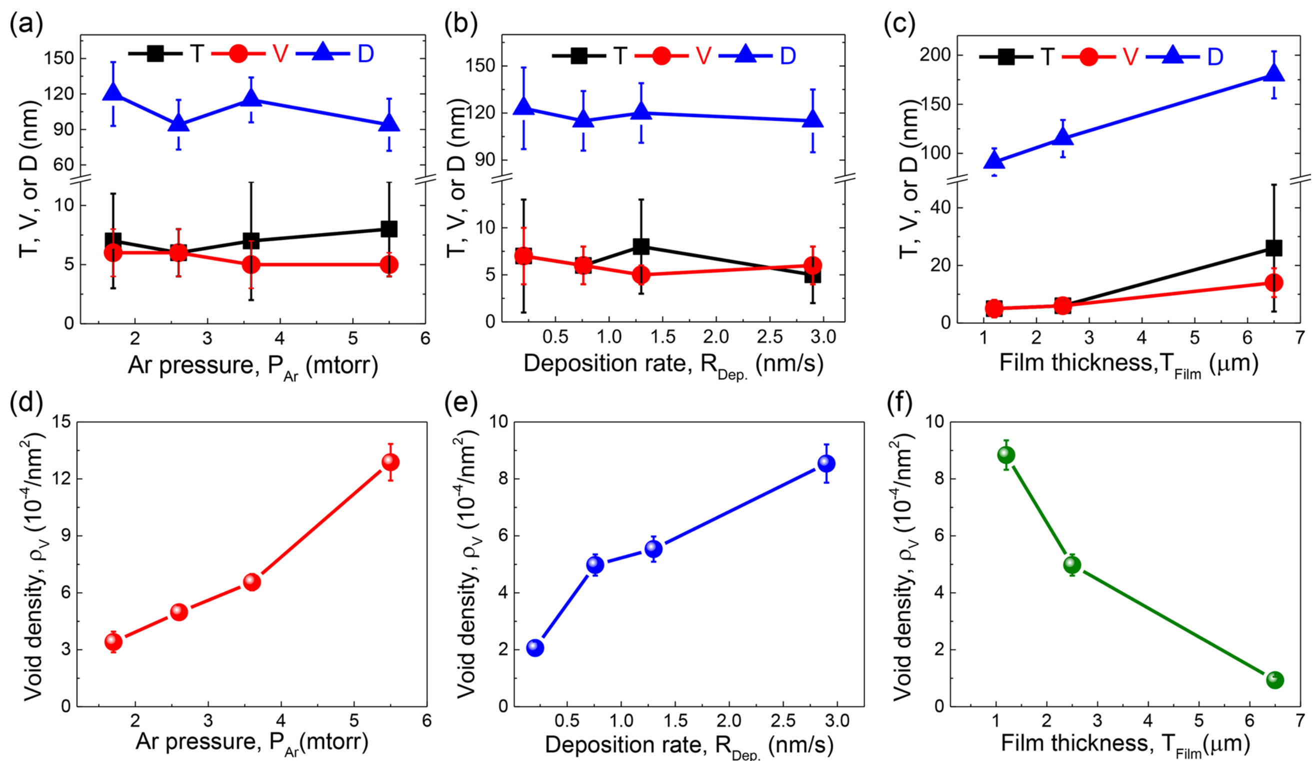

Fig. 5 **a**–**c** Variations of twin spacing T, void size V, and domain size D with increasing Ar pressure P_{Ar}, deposition rate $R_{Dep.}$, and film thickness T_{Flim}. **d**–**f** Void density ρ_V plotted as a function of deposition parameters

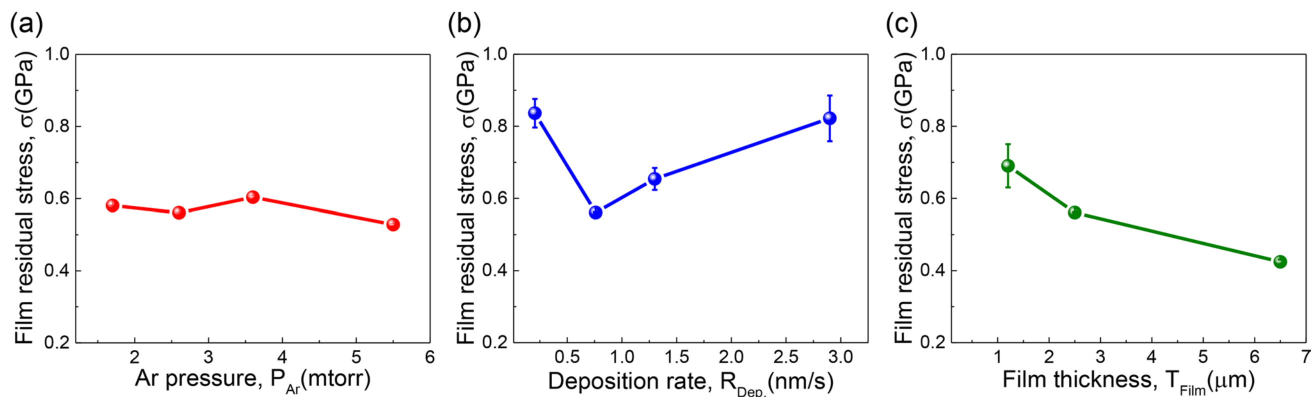

Fig. 6 Variation of film residual stress σ with increasing **a** Ar pressure P_{Ar}, **b** deposition rate $R_{Dep.}$, and **c** film thickness T_{Flim}

grain boundaries. Additionally, the polycrystalline Cu contains a much lower density of twin boundaries in contrast to the Type 1 NV–NT Cu films deposited on Si (110) (see Sect. 3.1).

3.3 Type 3: nanovoid–nanotwinned Cu (111) deposited on Si (111) with an Ag seed layer

The texture and microstructure of NV–NT Cu film can be regained on Si (111) substrate by adding a seed layer. For instance, Fig. 8 demonstrates an epitaxial Cu (111) deposited on Si (111) with an Ag seed layer (~ 200 nm thick). The XRD 2θ scan in Fig. 8a only shows the strong peaks of {111} planes, suggesting the epitaxial growth of Cu (111) on Ag/Si (111). The plan-view TEM micrograph in Fig. 8b shows the formation of nanovoids at domain boundaries, and the inset SAD pattern confirms the growth of epitaxial Cu (111) film. The cross-section TEM micrograph, together with the inset SAD pattern, in Fig. 8c reveals the formation of high-density growth twins in as-deposited NV–NT Cu (111) film.

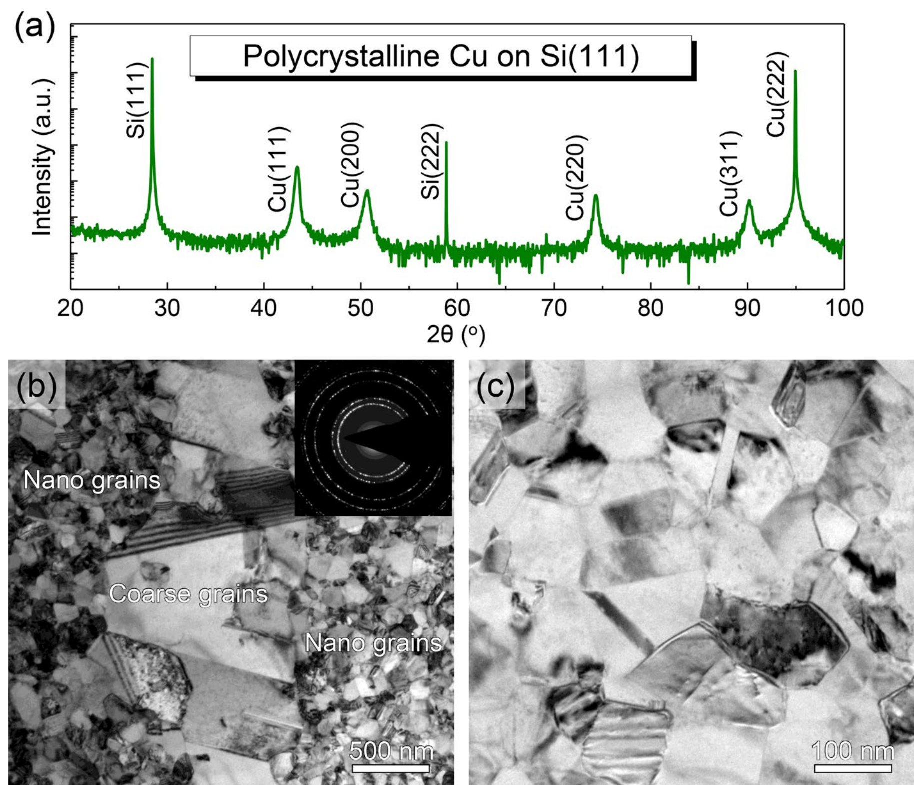

Fig. 7 The void-free polycrystalline Cu film directly deposited on Si (111) substrate. **a** 2θ XRD pattern showing diffraction peaks of Cu and Si. **b** The plan-view TEM micrograph of polycrystalline Cu with a bimodal grain size distribution. The inset SAD ring pattern in (**c**) suggests the formation of polycrystalline grains. **c** An enlarged view from the region with small nanograins

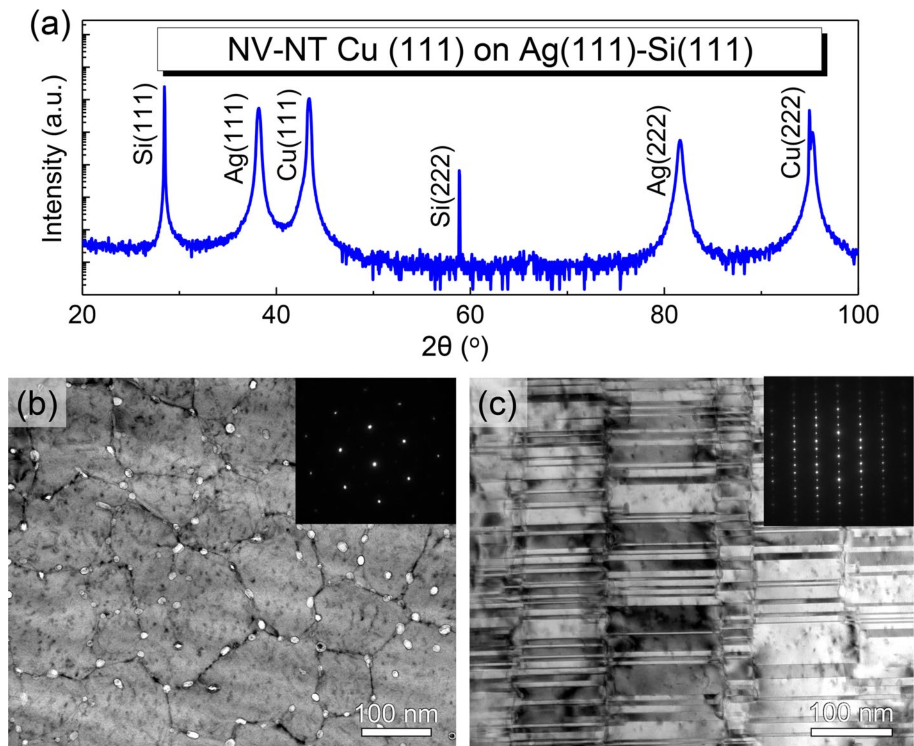

Fig. 8 The NV–NT Cu (111) film deposited on Si (111) substrate with an Ag seed layer (~200 nm thick). **a** 2theta-scan XRD spectra with (111)/(222) peaks of Cu, Ag, and Si. **b** Plan-view TEM micrograph showing the nanovoids at domain boundaries. **c** Cross-section TEM micrograph showing the nanotwins inside columnar domains

4 Discussion

The microstructural evolution during film deposition has been extensively studied, and the influence of deposition variables (e.g., deposition rate, Ar pressure) can be found in a number of reviews [3, 32–34]. It is generally recognized that a wide range of textures and microstructures can be developed in Cu films depending on preparation methods and conditions [35, 36]. In the current case of sputter-deposited NV–NT Cu (111), however, we found that varying deposition conditions alone can only modify the size, density, and distribution of microstructural features to some extent (see Sect. 3.1). The formation of nanovoids seems to be more strongly dependent on film texture (see Sects. 3.2 and 3.3). For this reason, in the following paragraphs, we will focus our attention on the influence of growth twins on the void formation in epitaxial Cu (111) film.

First, considering that the evolution of film microstructure is intimately related to the film growth process, we carefully inspected the growth front of NV–NT Cu film to obtain some hint of growth kinetics. As shown in Fig. 9a, the NV–NT Cu film surface exhibits 'island' configurations when observed from the top-down view. In addition, the cross-section (side view) TEM micrograph in Fig. 9b reveals a cycloid surface profile and a high density of the CTBs underneath the surface. The enlarged view in Fig. 9c shows small voids that are vertically aligned at the domain boundary. Such surface characteristics suggest that the boundary voids may form as columnar domains come into contact with each other. To reveal where the voids are nucleated along the columnar boundary, we further performed high-resolution TEM analysis. As shown in Fig. 10, there are three twins (Twins 1–3) separated by CTBs in the matrix. Also, there are two boundary voids, Voids 1 and 2 formed at the ends of Twin 1 and Twin 2, respectively. Between the voids, however, the matrix is almost joined with little spacing. It seems that the voids are likely to nucleate at the regions where the twin and matrix impinge. Based on these observations, we finally explain the growth of epitaxial NV–NT Cu (111) within the framework of island coalescence model [37]. According to this model, the film grows by the nucleation and coalescence of discrete islands when they come to impinge on each other [38, 39]. Also, this model predicts a large elastic strain in the film, which is in qualitative agreement with our experimental results in Fig. 6.

Following the island model, we can attribute the void formation to the increased energy barrier against coalescence when growth twins are present inside islands. The underlying mechanisms are illustrated schematically in Fig. 11. Here, we are first concerned with the microstructure of a polycrystalline Cu and attempt to understand why it is void-free. As shown in Fig. 11a1, when Cu is deposited onto Si (111) substrate, crystallites with random orientations $h_ik_il_i$ ($I = 1, 2, 3,$

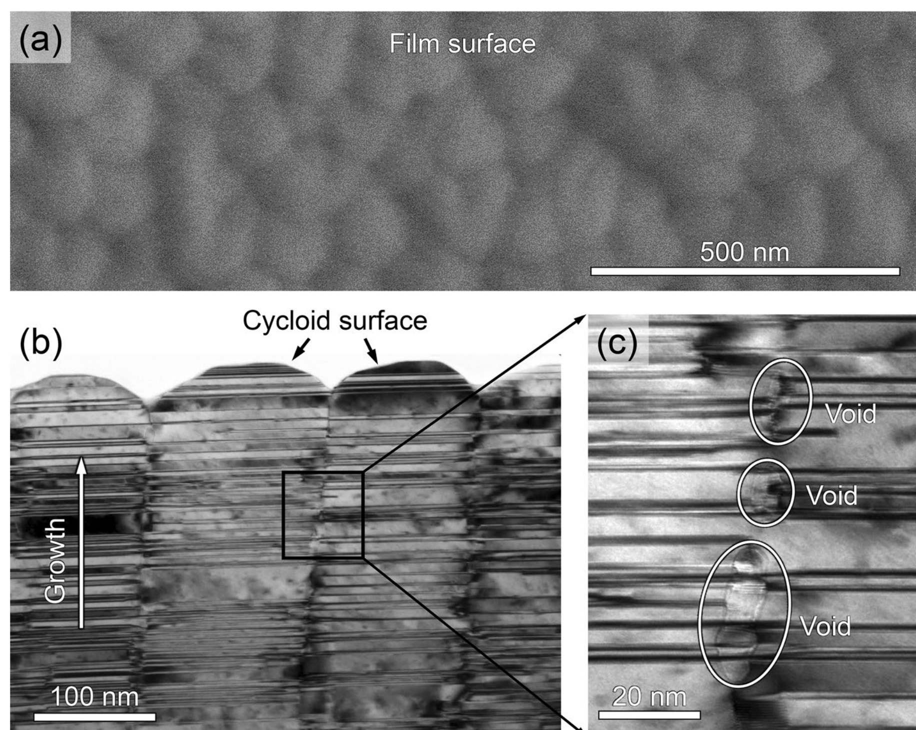

Fig. 9 Topography of film growth front of NV–NT Cu (111). The film is labeled as 'b2_1.3 nm/s' in Table 1. **a** SEM micrograph of the film surface. **b** Cross-section TEM micrograph of the film growth front with a cycloid surface. **c** Enlarged view of the boxed area in (**b**) demonstrating voids separately aligned along a domain boundary

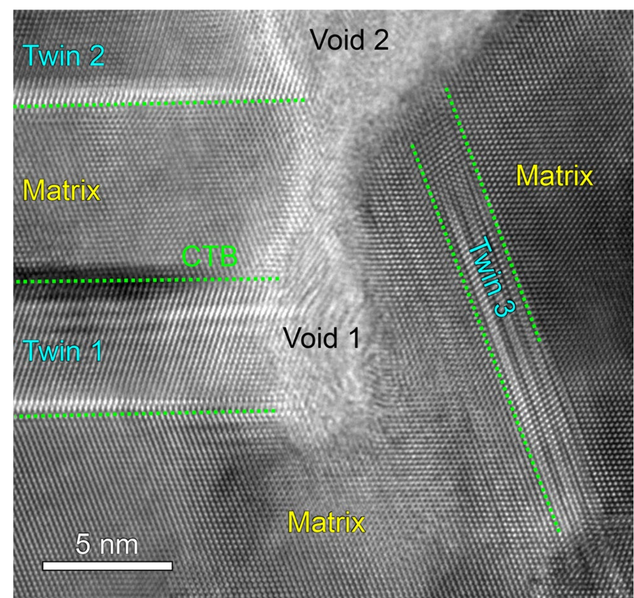

Fig. 10 High-resolution TEM micrograph of boundary voids in NV–NT Cu (111)

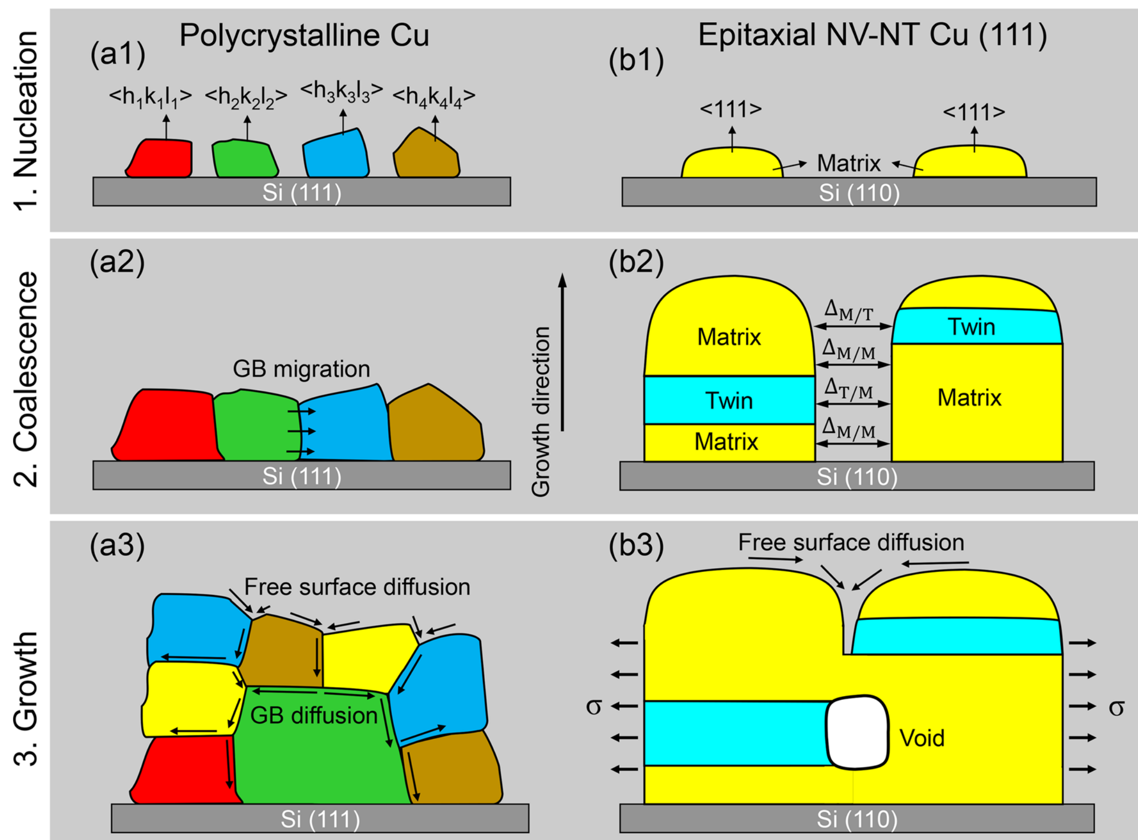

Fig. 11 Two-dimensional schematic representation of crystallite nucleation, coalescence, and growth in sputtered Cu films. **a1**–**a3** Formation of void-free polycrystalline Cu film on Si (111) substrate due to GB diffusion and migration. **b1**–**b3** Void formation mechanism through crystallite coalescence in epitaxial NT Cu (111) film on Si (110) substrate

4…) are initially nucleated. During deposition, these individual crystallites grow continuously until they coalescence into a continuous polycrystalline film, as schematically shown in Fig. 11a2. At this point the residual tensile stress might be very high, and some voids might also be formed due to the shadowing effects [40]. At the later stages of film growth,

however, the stress can be relaxed, and the voids can be removed by incorporating additional adatoms into grain boundaries through fast diffusions along surface—grain boundary network, as shown in Fig. 11a3. Meanwhile, grain boundary migration and secondary grain growth could be caused by local substrate heating. This process results in a bimodal grain size distribution, as observed in Fig. 7 or reported elsewhere [35, 41].

In comparison, when Cu is deposited onto Si (110), or onto Si (111) with an Ag seed layer, the individual crystallites are all preferentially <111>-orientated, as shown in Fig. 11b1. The orientation relationship could be determined by the geometrical lattice match rule [42]. As {111} is the twin plane for an FCC metal, and the growth twins are favored to nucleate on this plane for Cu due to its low stacking fault energy (45 mJ/m^2) [43, 44]. The crystallites, therefore, are composed of fine growth twins, as shown in Fig. 11b2. Although these twins and their matrix are oriented the same along the film growth direction, they have a large rotation angle (60°) in the film plane (twin plane). Hence, as the NT crystallites snap together on side walls, incoherent twin boundaries (ITBs) are expected to form at the intersections where twins meet the matrix, while at other locations where matrix faces matrix (or twin faces twin), no grain boundaries would form. The maximum gap size between adjoining crystallites can be estimated based on a simple energy criterion that the reduction of surface energy balances the increase of boundary energy and elastic energy [37]. For the twin-matrix segments, the maximum gap size Δ_{T-M} is described as [39]

$$\Delta_{T-M} = \left[2D\left(2\gamma_{sv} - \gamma_{ITB}\right)\frac{1-\upsilon}{E}\right]^{1/2} \tag{2}$$

where D is the crystallite (domain) size, E is the Young's modulus, υ is the Poisson's ratio, γ_{sv} is the surface energy, and γ_{ITB} is the incoherent twin boundary energy. For the matrix–matrix (or twin–twin) segments, the maximum gap size Δ_{M-M} (or Δ_{T-T}) is in the form of

$$\Delta_{M-M} = \left[4D\gamma_{sv}\frac{1-\upsilon}{E}\right]^{1/2} \tag{3}$$

Combining Eqs. (2) and (3), we can conclude that $\Delta_{M-M} > \Delta_{T-M}$, indicating that the joining between matrix and matrix (or twin and twin) is energetically favorable over the joining between twin and matrix. As a result, a void tends to nucleate at the twin–matrix intersection region when the regions below and above are ready to join (snap) together, as illustrated in Fig. 11b3. Upon nucleation, the void will be buried beneath the surface and is cut off from the surface diffusion. However, whether the buried void can remain intact thereafter also depends on the bulk diffusion. Note that, unlike the polycrystalline Cu that is composed of regular grain boundaries, the NT Cu (111) is dominated by CTBs, the special low-energy and high-coherent boundaries along which the diffusion is limited. Therefore, the buried void is able to survive the film growth, insomuch as the net diffusion into it is restricted.

The foregoing mechanism of void formation suggests that the NT Cu (111) film residual stress cannot be relaxed timely by incorporating additional adatoms. This is consistent with our experimental measurements. As shown in Fig. 6, all the sputtered NV–NT Cu have a large tensile stress ranging from 0.4 to 0.9 GPa. It has been pointed out that tensile stress might promote void nucleation and growth [45]. Consequently, more nanovoids are expected to form along domain boundaries provided that twins are present in the growing domains, as confirmed by our high-resolution TEM micrograph in Fig. 10. This mechanism also suggests that the void size and twin thickness should be comparable, as the formation of nanotwins precedes the nucleation of nanovoids. Indeed, Figs. 5a–c demonstrate that the twin size and void size are similar in most of the epitaxial NT Cu films regardless of the deposition conditions. The systematic studies presented here thus provide a practical method to manufacture NV–NT Cu. The discovery reported in epitaxial Cu may be applicable to other epitaxial NT metals.

5 Conclusion

Polycrystalline and epitaxial Cu thin films were synthesized by direct current magnetron sputtering deposition technique. The texture and microstructure of as-deposited films can be tailored by varying deposition conditions, changing orientation of Si substrate, or adding an Ag seed layer. The polycrystalline Cu film exhibits a typical bimodal distribution of grains with almost no nanovoids. In comparison, for the epitaxial Cu (111) films grown on Si (110) or on Si (111) with an Ag seed layer, their microstructures are characterized by high-density nanotwins and nanovoids. The nucleation of nanotwins inside columnar domains can be attributed to the low stacking fault energy of Cu, while the nucleation of

nanovoids at domain boundaries is caused by the high energy barrier at the twin-matrix intersections. The formation of these nanovoids in the epitaxial Cu films can be ascribed to the cutoff of surface diffusion and the restriction of bulk diffusion. Consequently, the nanovoid formation mechanism in NT Cu can be rationalized based on the proposed island coalescence model. This study suggests that texture and twin boundaries can play an important role in tailoring the formation of nanovoids in NT metals.

Acknowledgements We acknowledge financial support by Semiconductor Research Corporation (SRC) for supporting this work under Task 2878.017, managed by Center for Heterogeneous Integration Research in Packaging (CHIRP) and SRC. Xinghang Zhang also acknowledges financial support from NSF-DMR-2210152. Access to Materials Science Microscopy Center at Purdue University is also acknowledged. Cuncai Fan acknowledges financial support by City University of Hong Kong (project No. 9610627).

Author contributions CF carried out the experiment, wrote the main manuscript text, and prepared all figures. XZ and HW conceived of the idea, supervised the project, and edited the text. All authors reviewed the manuscript.

Data availability Data in the current study are available from the corresponding author, Cuncai Fan, upon reasonable request.

Declarations

Competing interests The authors declare no competing interests.

Open Access This article is licensed under a Creative Commons Attribution 4.0 International License, which permits use, sharing, adaptation, distribution and reproduction in any medium or format, as long as you give appropriate credit to the original author(s) and the source, provide a link to the Creative Commons licence, and indicate if changes were made. The images or other third party material in this article are included in the article's Creative Commons licence, unless indicated otherwise in a credit line to the material. If material is not included in the article's Creative Commons licence and your intended use is not permitted by statutory regulation or exceeds the permitted use, you will need to obtain permission directly from the copyright holder. To view a copy of this licence, visit http://creativecommons.org/licenses/by/4.0/.

References

1. Kelly PJ, Arnell RD. Magnetron sputtering: a review of recent developments and applications. Vacuum. 2000;56(3):159–72.
2. Freund LB, Suresh S. Thin film materials: stress, defect formation and surface evolution. Cambridge: Cambridge University Press; 2004.
3. Petrov I, Barna P, Hultman L, Greene J. Microstructural evolution during film growth. J Vac Sci Technol A Vac Surf Films. 2003;21(5):S117–28.
4. Thornton JA. The microstructure of sputter-deposited coatings. J Vac Sci Technol A Vac Surf Films. 1986;4(6):3059–65.
5. Tjong S, Chen H. Nanocrystalline materials and coatings. Mater Sci Eng R Rep. 2004;45(1–2):1–88.
6. Bufford DC, Wang YM, Liu Y, Lu L. Synthesis and microstructure of electrodeposited and sputtered nanotwinned face-centered-cubic metals. MRS Bull. 2016;41(4):286–91.
7. Zhang X, Anderoglu O, Hoagland R, Misra A. Nanoscale growth twins in sputtered metal films. JOM. 2008;60(9):75–8.
8. Li Q, Xue S, Fan C, Richter NA, Zhang Y, Chen Y, Wang H, Zhang X. Epitaxial nanotwinned metals and alloys: synthesis-twin structure–property relations. CrystEngComm. 2021;23(38):6637–49.
9. Lu K. Stabilizing nanostructures in metals using grain and twin boundary architectures. Nat Rev Mater. 2016;1(5):1–13.
10. Sansoz F, Lu K, Zhu T, Misra A. Strengthening and plasticity in nanotwinned metals. MRS Bull. 2016;41(4):292–7.
11. Anderoglu O, Misra A, Wang H, Ronning F, Hundley M, Zhang X. Epitaxial nanotwinned Cu films with high strength and high conductivity. Appl Phys Lett. 2008;93(8): 083108.
12. Lu L, Shen Y, Chen X, Qian L, Lu K. Ultrahigh strength and high electrical conductivity in copper. Science. 2004;304(5669):422–6.
13. Anderoglu O, Misra A, Wang H, Zhang X. Thermal stability of sputtered Cu films with nanoscale growth twins. J Appl Phys. 2008;103(9): 094322.
14. Zhang X, Misra A. Superior thermal stability of coherent twin boundaries in nanotwinned metals. Scr Mater. 2012;66(11):860–5.
15. Zhao Y, Furnish TA, Kassner ME, Hodge AM. Thermal stability of highly nanotwinned copper: the role of grain boundaries and texture. J Mater Res. 2012;27(24):3049–57.
16. Li J, Xie D, Xue S, Fan C, Chen Y, Wang H, Wang J, Zhang X. Superior twin stability and radiation resistance of nanotwinned Ag solid solution alloy. Acta Mater. 2018;151:395–405.
17. de Bellefon GM, Robertson I, Allen T, van Duysen J-C, Sridharan K. Radiation-resistant nanotwinned austenitic stainless steel. Scr Mater. 2019;159:123–7.
18. Shang Z, Niu T, Sun T, Xue S, Fan C, Chen W-Y, Li M, Wang H, Zhang X. In situ study on radiation response of a nanotwinned steel. Scr Mater. 2022;220: 114920.
19. Yu K, Fan C, Chen Y, Li J, Zhang X. Recent studies on the microstructural response of nanotwinned metals to in situ heavy ion irradiation. JOM. 2020;72:160–9.
20. Zhang X, Wang H, Chen X, Lu L, Lu K, Hoagland R, Misra A. High-strength sputter-deposited Cu foils with preferred orientation of nanoscale growth twins. Appl Phys Lett. 2006;88(17): 173116.

21. Lu L, Chen X, Huang X, Lu K. Revealing the maximum strength in nanotwinned copper. Science. 2009;323(5914):607–10.
22. Hu Z, Du J, Wang P, Wang X, Zhang Y, Qiu Y, Fu E. Insight into the impact of nanovoids on the electrical and mechanical properties of nanotwinned copper films. Scr Mater. 2017;137:41–5.
23. Ma H, Zou Y, Sologubenko AS, Spolenak R. Copper thin films by ion beam assisted deposition: strong texture, superior thermal stability and enhanced hardness. Acta Mater. 2015;98:17–28.
24. Fan C, Li Q, Ding J, Liang Y, Shang Z, Li J, Su R, Cho J, Chen D, Wang Y. Helium irradiation induced ultra-high strength nanotwinned Cu with nanovoids. Acta Mater. 2019;177:107–20.
25. Fan C, Chen Y, Li J, Ding J, Wang H, Zhang X. Defect evolution in heavy ion irradiated nanotwinned Cu with nanovoids. J Nucl Mater. 2017;496:293–300.
26. Chen Y, Yu KY, Liu Y, Shao S, Wang H, Kirk M, Wang J, Zhang X. Damage-tolerant nanotwinned metals with nanovoids under radiation environments. Nat Commun. 2015;6(1):1–8.
27. Fan C, Annadanam RGS, Shang Z, Li J, Li M, Wang H, El-Azab A, Zhang X. Irradiation induced void spheroidization, shrinkage and migration in Cu at elevated temperatures: an in situ study. Acta Mater. 2020;201:504–16.
28. Fan C, Sreekar A, Shang Z, Li J, Li M, Wang H, El-Azab A, Zhang X. Radiation induced nanovoid shrinkage in Cu at room temperature: an in situ study. Scr Mater. 2019;166:112–6.
29. Stoney GG. The tension of metallic films deposited by electrolysis. Proc R Soc Lond Ser A Contain Pap Math Phys Charact. 1909;82(553):172–5.
30. Hopcroft MA, Nix WD, Kenny TW. What is the Young's modulus of silicon? J Microelectromech Syst. 2010;19(2):229–38.
31. Lloyd J, Nakahara S. Voids in thin as-deposited gold films prepared by vapor deposition. J Vac Sci Technol. 1977;14(1):655–9.
32. Messier R, Giri A, Roy R. Revised structure zone model for thin film physical structure. J Vac Sci Technol A Vac Surf Films. 1984;2(2):500–3.
33. Barna P, Adamik M. Fundamental structure forming phenomena of polycrystalline films and the structure zone models. Thin Solid Films. 1998;317(1–2):27–33.
34. Mahieu S, Ghekiere P, Depla D, De Gryse R. Biaxial alignment in sputter deposited thin films. Thin Solid Films. 2006;515(4):1229–49.
35. Tracy D, Knorr D. Texture and microstructure of thin copper films. J Electron Mater. 1993;22(6):611–6.
36. Kateb M, Gudmundsson JT, Brault P, Manolescu A, Ingvarsson S. On the role of ion potential energy in low energy HiPIMS deposition: an atomistic simulation. Surf Coat Technol. 2021;426: 127726.
37. Hoffman R. Stresses in thin films: the relevance of grain boundaries and impurities. Thin Solid Films. 1976;34(2):185–90.
38. Misra A, Nastasi M. Evolution of tensile residual stress in thin metal films during energetic particle deposition. J Mater Res. 1999;14(12):4466–9.
39. Nix W, Clemens B. Crystallite coalescence: a mechanism for intrinsic tensile stresses in thin films. J Mater Res. 1999;14(8):3467–73.
40. Smith RW, Srolovitz DJ. Void formation during film growth: a molecular dynamics simulation study. J Appl Phys. 1996;79(3):1448–57.
41. Simões S, Calinas R, Vieira M, Vieira M, Ferreira PJ. In situ TEM study of grain growth in nanocrystalline copper thin films. Nanotechnology. 2010;21(14): 145701.
42. Jiang H, Klemmer T, Barnard J, Payzant E. Epitaxial growth of Cu on Si by magnetron sputtering. J Vac Sci Technol A Vac Surf Films. 1998;16(6):3376–83.
43. Zhang X, Misra A, Wang H, Shen T, Nastasi M, Mitchell T, Hirth J, Hoagland R, Embury J. Enhanced hardening in Cu/330 stainless steel multilayers by nanoscale twinning. Acta Mater. 2004;52(4):995–1002.
44. Kateb M, Gudmundsson JT, Ingvarsson S. Effect of substrate bias on microstructure of epitaxial film grown by HiPIMS: an atomistic simulation. J Vac Sci Technol A. 2020;38(4): 043006.
45. Braski D, Schroeder H, Ullmaier H. The effect of tensile stress on the growth of helium bubbles in an austenitic stainless steel. J Nucl Mater. 1979;83(2):265–77.

Publisher's Note Springer Nature remains neutral with regard to jurisdictional claims in published maps and institutional affiliations.